Reviews

Structure and properties of nanostructured films based on refractory compounds

R. A. Andrievskii and G. V. Kalinnikov*

Institute of Problems of Chemical Physics, Russian Academy of Sciences,
1 prosp. Akad. Semenova, 142432 Chernogolovka, Moscow Region, Russian Federation.
Fax: +7 (496) 522 3507. E-mail: ara@icp.ac.ru

The results of studies of the structure and physicochemical properties of nanostructured films based on refractory carbides, borides, and nitrides are generalized. The possibility to obtain diamond-level hardness values is considered. The thermal stability of the hardness and the nanostructure of the films is discussed. The phase diagrams of refractory compounds in the nanocrystalline state are considered. The results of high-temperature oxidation of nanocrystalline and amorphous films are described.

Key words: nanostructured films, carbides, borides, nitrides, hardness, thermal stability, nanostructure, phase diagram, oxidation of films.

In recent years, the design of novel promising materials has been increasingly focused on the nanostructure approach based on the use of the advantages of nanostructure according to which the size of the major structural units (grains, phase inclusions, layers, pores, *etc*.) is in the range from 1—2 to ~100 nm. The possibility of producing diverse materials with high levels of physicochemical and physicomechanical properties provided by nanostructure attracts the attention of scientists and engineers. This is obvious from both the considerable expansion of the research and design works related to nano problems and the pronounced increase in the information flow (see, for example, Refs 1 and 2).

Refractory compounds are carbides, borides, nitrides, oxides, and other phases with melting points higher than 2000 °C.[3] They form the basis of many technologically important materials for which transition to the nanocrystalline state can be accompanied by considerable enhancement of their characteristics. The lack of sufficient data on this topic (as compared with the information for metals and alloys) was emphasized in reviews.[4,5] It was of scientific and practical interest to elucidate the effect of the crystallite size on the hardness, electrical resistance, and other properties and on the change in the phase diagrams and the behavior of nanostructures upon oxidation. The choice of films as investigation objects was dictated by the possibility to use pore-free samples with lower impurity contents and with broad grain size ranges, which is hardly practicable in the case of powder production techniques.[6] Moreover, films of refractory compounds are of interest by

Published in Russian in *Izvestiya Akademii Nauk. Seriya Khimicheskaya,* No. 6, pp. 1001—1007, June, 2011.

1066-5285/11/6006-1025

themselves for many applied fields (mechanical engineering, power engineering, electronics, *etc.*).

In our works, multilayer nitride films were prepared in nitrogen plasma by vacuum arc deposition,[7,8] and single-layer films based on borides, nitrides, and carbides were obtained by non-reactive magnetron sputtering.[9]

Hardness. Thermal stability

The effect of the number of layers in the multilayer TiN/NbN, TiN/ZrN, and TiN/CrN films on their microhardness (H_V) is illustrated in Fig. 1; the total thickness of all films was the same and equal to 2 μm.[7,8] From these data, it is quite obvious that H_V considerably increases with a decrease in the layer thickness (*i.e.*, with an increase in the number of layers) and, hence, with an increase in the number of interfaces, which serve as locks in the dislocation and crack propagation. The non-monotonic change in H_V for the TiN/CrN films is caused by the formation of a solid solution, (Ti,Cr)N, in the TiN—CrN system (the lowest-temperature system compared with TiN—NbN and TiN—ZrN). This was detected by powder X-ray diffraction and confirms the crucial locking function of interfaces. The strengthening caused by the formation of the solid solution is less efficient for the enhancement of hardness than the effect of interfaces.

Note that the diamond-level hardness characteristics were first obtained almost at the same time by several independently working research teams (Austria, former-USSR, USA, Germany, and Sweden), who studied single- and multi-layer films based on nitrides, borides, and carbides (Table 1). In all probability, the decrease in the hardness of multilayer TiN/VN films at a monolayer thickness of <3 nm (see Ref. 13) is also caused by disappearance of interfaces as a result of mutual heterodiffusion and formation of the (Ti,V)N solid solution.

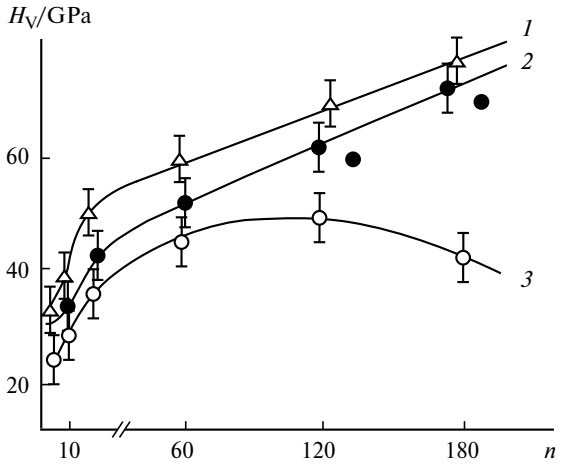

Fig. 1. Variation of the microhardness (H_V) of multilayer nitride films *vs.* the number of layers (n): TiN/NbN (*1*), TiN/ZrN (*2*), TiN/CrN (*3*).[8]

Table 1. Single- and multi-layer films based on refractory compounds with hardness at the level of superhard materials

Compound	Microhardness /GPa (δ/nm)*	Reference
	Single-layer films	
$Ti(B,C,N)_X$	~70	10
$Ti(B,C,N)_X$	~60	11
B_4C	50—70	12
	Multilayer films	
TiN/VN	54 (3)	13
TiN/NbN	~50 (100) ~78 (11)	7, 8
TiN/NbN	48	14
TiN/ZrN	~44 (100) ~70 (11)	7, 8

* δ is the monolayer thickness; the total film thickness is 2—3 μm.

A non-monotonic variation of hardness as a function of the nanocrystallite size (L) was also observed for boron nitride samples prepared at high pressures and temperatures (16—20 GPa, 1500—1900 °C).[15] The maximum hardness was found at $L = 14\pm2$ nm ($H_V = 85\pm5$ GPa) for an aggregated nanocomposite (two-phase structure of sphalerite and wurtzite BN modifications) and at $L \approx 40$ nm ($H_V = 59\pm3$ GPa) for the sphalerite BN modification. This variation is similar to the situation observed for nanometals,[16] although its nature requires further investigation.

High hardness values at a ~100 GPa level were obtained for nanocomposite TiN/Si_3N_4 films,[17] but only a few researchers were able to reproduce these results. In a review,[18] data on these films were analyzed in detail and the deviations of the results were attributed to the difficulty of maintaining the equilibrium nitrogen pressure during the production of films and to the effect of oxygen impurities.

The evolution of hardness and other properties of single-layer films based on TiB_2—TiN and TiB_2—B_4C systems was studied with allowance for the effect of additional external magnetic field (AEMF) and of the temperature annealing.[9,19—23] Tables 2 and 3 present some of these data.

The obtained results can be briefly summarized as follows:

— The application of AEMF during the magnetron sputtering of two- and three-component boride, nitride, and carbide films is accompanied by a decrease in the grain size and an increase in the hardness. This is observed not only for crystalline films but also for amorphous objects. Analysis showed also that these changes are attributable to higher concentration of the plasma discharge near the substrate and, hence, higher concentration of the de-

Table 2. Composition, structure, average grain size (L), and microhardness (H_V) of the films sputtered without AEMF (I) and with application of AEMF (II) (induction of 0.04 T)[20]

Target (wt.%)	Approximate formula[a]	Structural type	I		II	
			L/nm	H_V/GPa	L/nm	H_V/GPa
TiB_2	$Ti(B_{0.73}N_{0.2}O_{0.05}C_{0.02})_{1.56}$	AlB_2	3.6±1.8	32—39	3.3±1.1	42—48
TiB_2+TiN(25)	$Ti(B_{0.56}N_{0.29}O_{0.05}C_{0.1})_{1.32}$	AlB_2	2.3±1.1	28—34	—[b]	44—48
TiB_2+TiN(50)	$Ti(B_{0.36}N_{0.42}O_{0.15}C_{0.07})_{1.56}$	NaCl	2.9±1.5	31—36	1.8±0.3	52—58
TiB_2+TiN(75)	—[b]	NaCl	5.9±4.0	25—30	6.5±2.3	44—49
TiN	$Ti(N_{0.6}O_{0.2}C_{0.2})_{1.58}$	NaCl	29±15	23—28	8.8±2.2	36—42
TiB_2+B_4C(25)	—[b]	AlB_2	8.5±4.0	40—46	2.9±0.3	54—58
TiB_2+B_4C(50)	—[b]	Amorphous structure	—	44—50	—	60—68
TiB_2+B_4C(75)	—[b]	The same	—	46—54	—	62—71
B_4C	—[b]	The same	—	42—50	—	48—56

[a] According to layer-by-layer Auger analysis.
[b] Not determined.

posited ions, which, in turn, affects the increase in the number and the growth rate of crystallization centers.[21] In addition, by decreasing the grain size, AEMF also narrows down the grain size distribution.

— As shown by powder X-ray diffraction and atomic force microscopy studies of the films, the application of AEMF induces a change in the texture of crystalline films and decreases the surface roughness.

— According to the estimate of the averaged chemical composition of the films by the Auger spectroscopy data (TiB_2—TiN system),[9] the films are superstoichiometric and contain oxygen, nitrogen, and carbon impurities. The use of Rutherford backscattering spectroscopy for the TiB_2—B_4C system revealed that application of AEMF decreases the carbon concentration in the films.[22]

— A study of the electrical and galvanomagnetic properties of the TiN films with different grain size (L = 29±15 and 8.8±2.2 nm) showed that the distribution of oxygen and carbon impurities within the grains and at the grain boundaries can be regarded as virtually homogeneous and that the conductivity of these films upon a decrease in the grain size is determined by only the mobility of carriers (electrons), which decreases through their scattering at the crystallite interfaces, and the number of carriers does not depend on the grain size.[23]

— The thermal stability of the films was studied in many works (see, for example, Refs 7, 18—20, 24—26). It can be seen from Table 3 (the data for the initial films are given in Table 2) that a pronounced change in the hardness of single-layer TiB_2—TiN films starts at ~1000 °C. Multilayer films are more thermally stable.[7,24—28] Note that their thermal stability increases with a decrease in the layer thickness (Fig. 2).[26] This situation related to the specific features of free energy variation in nanomaterials was described in detail in a review.[25] An example of unusual variation of the hardness during the annealing is observed in films based on systems susceptible to spinodal

Table 3. Effect of the temperature of annealing (T_{ann}) for 15 min on the grain size (L) and microhardness (H_V) of the TiB_2—TiN films (1—2 μm thick)[19]

Target (wt.%)	T_{ann} = 700 °C		T_{ann} = 1000 °C	
	L/nm	H_V/GPa	L/nm	H_V/GPa
TiB_2	—*	40—46	—*	35—39
TiB_2—TiN(25)	4.4±1.4	40—45	—*	32—38
TiB_2—TiN(50)	3.7±1.2	47—54	3.4±1.9	38—45
TiB_2—TiN(75)	8.1±4.4	52—58	7.9±3.8	32—42
TiN	13.0±6.6	38—42	10±7.0	33—40

* Not determined.

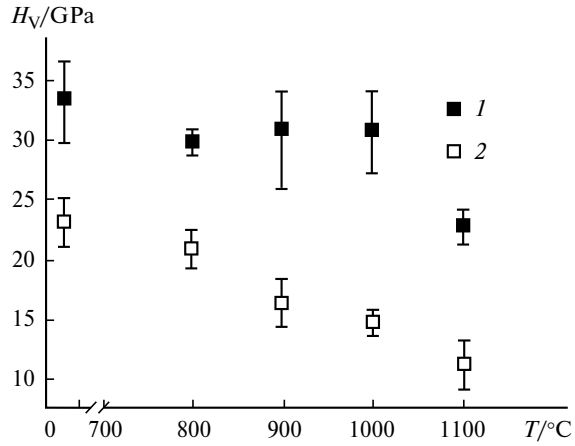

Fig. 2. Microhardness (H_V) of multilayer TiN/AlN films *vs.* annealing temperature under argon for 2 h. The total film thickness is 300 nm; the thickness of individual layers is 2.9 (*1*) and 16 nm (*2*)[26].

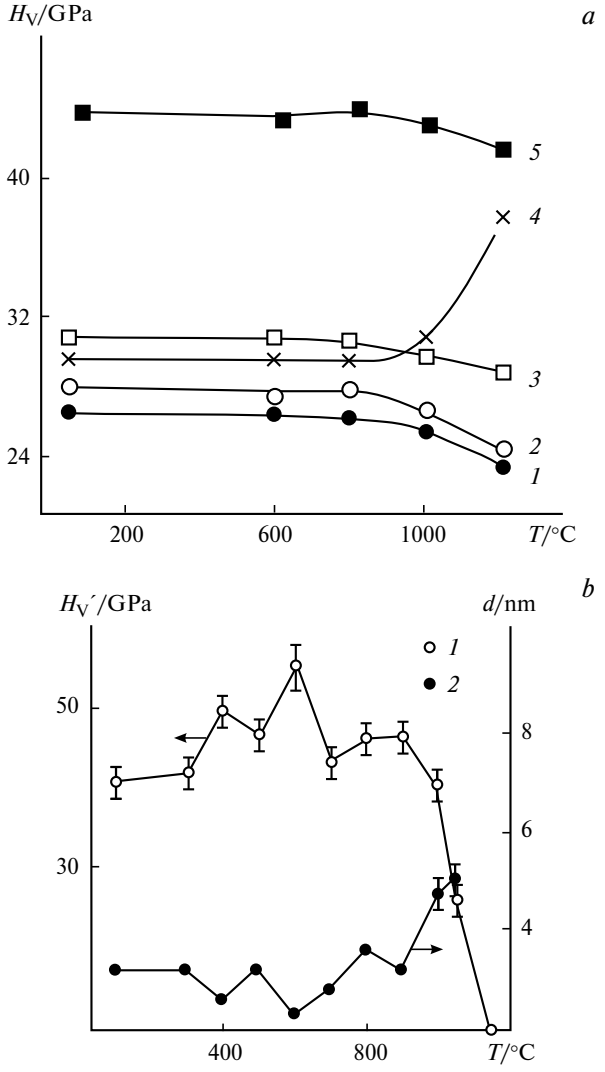

Fig. 3. Effect of the annealing temperature on the hardness of films based on TiN—ZrN (*a*: ZrN (*1*), TiN (*2*) systems, ten-layer TiN/ZrN film (*3*), doped (Ti,Zr)N film (*4*), twenty-layer TiN/ZrN film (*5*)),[7] and TiN—AlN (in the amorphous Si_3N_4 matrix) (*b*: hardness (*1*), grain size (*2*)).[18]

decomposition, as shown in Fig. 3 for (Ti,Zr)N and (Ti,Al)N—Si_3N_4 films. At high temperatures, single-phase TiN—ZrN and TiN—AlN systems decompose to give nanodispersed phases, which induces an increase in the hardness as the annealing temperature is raised. Films based on these systems represent a peculiar example of so-called smart materials, which not only do not lose their properties, including hardness, during operation but can even improve them somewhat.

— Analysis of the obtained results also showed that the unambiguous relation between the hardness and the grain size cannot always be followed (see Tables 2 and 3), because the properties of the nanomaterials are determined, apart from the grain size, by many other factors (state of grain boundaries, impurities and their segregation, grain shape, residual stresses, *etc.*). The role of size effect and interfaces in the formation of properties of nanomaterials (in particular, films as typical nanomaterials) was described in detail in reviews.[29,30]

Evolution of phase diagrams in the nanorange

The general characteristics of the effect of the ultradisperse state on the shift of phase equilibria in heterophase systems (in particular, in the Zr—C system) were presented in monographs.[31,32] It was of interest to consider this issue as applied to nanocomposites based on refractory compounds. It is known[3] that TiB_2—TiN (TiC), TiB_2—B_4C, and TiN—AlN pseudobinary diagrams are of eutectic type with minor mutual solubility of components in the solid state. Previously, we attempted to evaluate the type of these diagrams considering the component dispersity.[4,21,25,33,34] Using the expressions for the partial free energies of the system in the liquid and solid states (in the latter case, the excess component of the grain-boundary surface energy was included) in the simplest approximation of the theory of regular solutions, the relations that reflect the effect of the component dispersity, for example, on the decrease in the eutectic temperature ΔT_E were obtained:

$$\Delta T_E = \Delta G_2/(R\ln x), \quad \text{(I)}$$

$$\Delta T_E = \Delta G_2/(R\ln x_E - \Delta S_{M_2}), \quad \text{(II)}$$

$$\Delta T_E = \Delta G_1/[(1 - x_E)/(1 - x) - \Delta S_{M_1}], \quad \text{(III)}$$

where ΔG_i is the contribution of the excess grain-boundary surface energy per mole, $\Delta G_i = 6V_i\sigma_i/L_i$, V_i is the molar volume, σ_i is the grain-boundary surface energy, x and x_E are the concentrations of the limiting solubility and eutectics, respectively, ΔS_{Mi} is the entropy of melting and L_i is the inclusion (grain) size.

Relations (I)—(III) are equivalent, and their practical application depends on the presence of specific data for components 1 and 2. Tables 4—6 summarize the calculated ΔT_E and T_E values for the TiB_2—TiN, TiB_2—TiC, TiB_2—B_4C, and TiN—AlN systems. It can be seen from these data that an appreciable decrease in the eutectic temperature may occur when the size of the disperse component is of the order of several tens of nanometers. No data on the grain-boundary surface energy for these systems are available, and Table 6 presents the results for three probable σ_i values (the data of Tables 4 and 5 refer to $\sigma_i = 3$ J m^{-2}). Taking account of the phase composition of the films for the TiB_2—TiN system (see Table 2), the dashed lines in Fig. 4 show the approximate diagram of this system for film samples with a grain size of ~10 nm; for comparison, the equilibrium diagram is also given.[3,34]

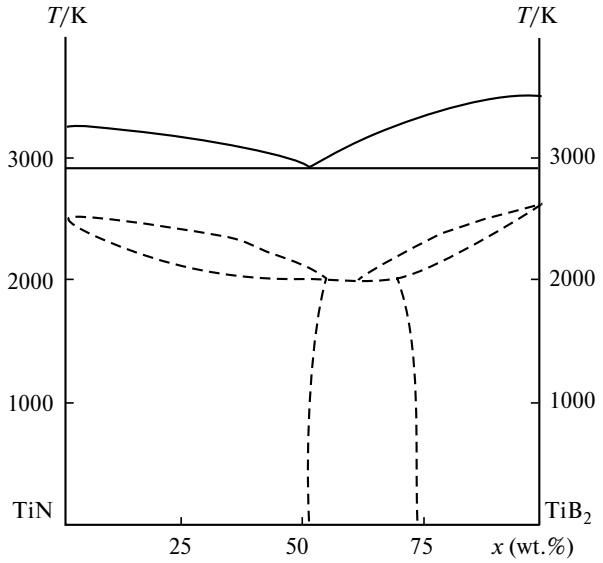

Fig. 4. Phase diagram TiN—TiB_2 for coarsely crystalline (solid lines) and film (dashed lines) samples (grain size ~10 nm);[34] x is the weight fraction of TiB_2 in the system.

Of course, one should bear in mind that the performed calculations are rough, which is due to both limitations of the regular solution approach and the uncertainty in the σ values. Nevertheless, these calculations may be very useful for estimating the top operating temperatures in the design of refractory materials based on nanocrystalline refractory compounds.

Table 4. Decrease in the eutectic temperature (ΔT_E) for the pseudobinary systems TiB_2—TiN(TiC) and TiN(TiC)—TiB_2 at different dispersity of the second component[9,25] *

L/nm	ΔT_E/K	
	TiB_2—TiN(TiC)	TiN(TiC)—TiB_2
200	35	45
100	70	90
20	350	450
10	700	900

* For coarse-grain TiB_2—TiC and TiB_2—TiN samples, T_E values are 2790 and 2870 K, respectively.[3]

Table 5. Eutectic temperature T_E for the pseudobinary system TiN—AlN at different grain size (L) of the components*

L/nm	T_E/K		
	TiN	AlN	TiN, AlN
200	2660	2710	2650
100	2610	2690	2590
20	2160	2565	2110

* For coarse-grain samples, T_E = 2715 K.[33]

Table 6. Decrease in the eutectic temperature (ΔT_E) for the system TiB_2—B_4C in films with different grain size (L) at different grain-boundary surface energy (σ)[21] *

σ/J m^{-2}	ΔT_E/K	
	L = 5 nm	L = 10 nm
3	1000	500
2	670	340
1	340	170

* For coarse-grain samples, T_E = 2580 K.

Oxidation of nanocomposite films

High-temperature oxidation of film nanocomposites based on AlN was considered in a study that we performed together with Ukrainian and French specialists.[35] Figure 5 shows the DTA and DTG curves for oxidation of the films obtained by non-reactive magnetron sputtering on the following targets (wt.%): AlN+TiN(50) (film **1**), AlN+TiB_2(50) (film **2**), and AlN+TiB_2(10)+SiC(20) (film **3**). It can be seen from these data that under the heating conditions applied (15 °C min^{-1}), noticeable oxidation of films **1**—**3** starts at ~750, ~950, and ~1020 °C, respectively. The temperatures of the onset of vigorous oxidation are arranged in the same order (~1100, ~1200, and ~1300 °C), film **3** being most resistant against oxidation. Comparison of the presented results with the data for coarsely crystalline samples oxidized under the same conditions showed that the specific weight gain on oxidation is 4—5 times lower for film samples. This interesting conclusion deserves special discussion.

The key reactions that may occur during the oxidation of films **1**—**3** are given below in the general form.

1

$$2\,(Ti_{1-y}Al_y)N_x + (2 - y/2)\,O_2 \rightarrow \rightarrow 2(1 - y/2)\,TiO_2 + y\,Al_2O_3 + x\,N_2 \quad (1)$$

$$TiO_2 + Al_2O_3 \rightarrow Al_2TiO_5 \quad (2)$$

2

$$2\,TiB_2 + 5\,O_2 \rightarrow 2\,TiO_2 + 2\,B_2O_3 \quad (3)$$

$$4\,AlN + 3\,O_2 \rightarrow 2\,Al_2O_3 + 2\,N_2 \quad (4)$$

$$2\,Al_2O_3 + B_2O_3 \rightarrow Al_4B_2O_9 \quad (5)$$

$$9\,Al_2O_3 + 2\,B_2O_3 \rightarrow Al_{18}B_4O_{33} \quad (6)$$

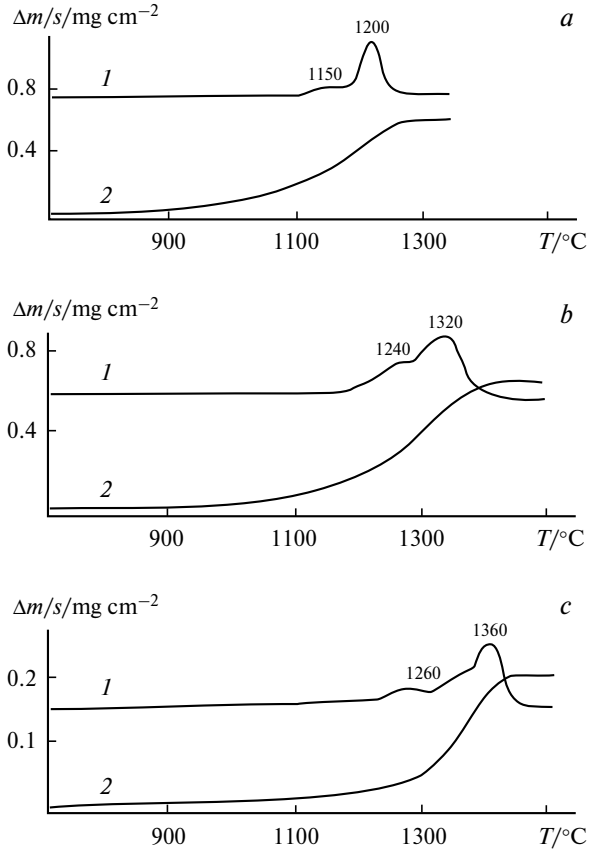

Fig. 5. DTA (*1*) and TGA (*2*) curves for the oxidation of AlN—TiN(50) (*a*), AlN—TiB_2(50) (*b*), and AlN—TiB_2(10)—SiC(20) (*c*) films.[35]

3

$$SiC + 2\ O_2 \rightarrow SiO_2 + CO_2 \quad (7)$$

$$3\ Al_2O_3 + 2\ SiO_2 \rightarrow 3\ Al_2O_3 \cdot 2\ SiO_2 \quad (8)$$

In addition, reaction (2) proceeds for film **2** and reactions (2)—(6) occur for film **3**.

This list of reactions does not take into account the possible effect of impurities (for example, iron, the presence of which is related to powder grinding for production of the targets), the formation of non-stoichiometric phases, and reactions with nitrogen. It is obvious from general considerations that high-temperature interaction of these films with air is a multistage process. The initial step of oxidation of almost any film involves the formation of rutile and (in the case of films **2** and **3**) boron oxide layers. In view of the known data on the oxidation of coarsely crystalline objects of a similar composition, the DTA peak at 1200 °C (film **1**) can be attributed to reaction (2), while peaks at 1240 and 1320 °C (film **2**) correspond, most likely, to reactions (5), (6), and (2). For film **3**, the peaks at 1260 and 1390 °C are caused by reactions (7) and (4) to give β-cristobalite and α-alumina, respectively; the peak at 1390 °C corresponds also to solid-state reactions (2) and (8) giving aluminum titanate and mullite, respectively. The last-mentioned two reactions determine apparently the composition of the protecting layer on film **3**. Since the films are thin and the number of phases formed, for example, by reactions (5) and (6), is rather small, the phase composition is only partly confirmed by powder X-ray diffraction data.

The data of X-ray spectral microanalysis obtained by scanning of 0.2 mm-long areas on the film surface confirm the presence of a phase with composition resembling aluminum titanate for films **1**—**3**. Energy-dispersive analysis revealed enrichment of the surface layers with aluminum and depletion in titanium, while the scanning electron microscopy fractography analysis of the films identified the presence of columnar nanoinclusions in the nanocrystalline matrix with characteristic sizes of ~100 nm; these inclusions were found only in film **3**. In films **1** or **2**, no columnar inclusions were found and the size of the structural components after oxidation was 300—600 nm.

Thus, high scaling resistance characteristics for film **3** can be explained by surface enrichment with aluminum with the formation of a stable protecting layer. Crystallization of the columnar inclusions favors the retention of the nanocrystalline structure and higher diffusion mobility. It is customarily believed that due to the presence of numerous interfaces, nanocrystalline materials have higher diffusion mobility (permeability) and, hence, lower corrosion resistance than conventional coarsely crystalline objects.[36] However, in our case, one can reasonably assume that the nanostructure provided the mobile formation of a stable protecting layer. This standpoint is confirmed by the results of a study[37] in which a higher scaling resistance was found for the nanocrystalline Fe—Cr(10) alloy with L = 52 nm than for the same microcrystalline alloy with L = 1.5 μm. A higher content of chromium (and protecting Cr_2O_3 film) for the nanocrystalline alloy was confirmed by independent methods.

The oxidation resistances of films based on simple and complex refractory compounds (TiC, TiN, (Ti,Al)N, (Ti,Al,Cr)N, Mo(N,Si), Ti(N,Si), *etc*.) were compared in detail.[38] Whereas for the nanocrystalline films based on titanium compounds, the upper temperature limit of application is about ~1000 °C, for silicon-based amorphous films, the temperature limit increases by ~500 °C, and Si—B—C—N-based films supported on sapphire and silicon carbide are stable at 1700 °C.

***

It should be emphasized that the problems of nanostructured coatings, in particular, technology, strength, physical properties, radiation resistance, simulation, and applications were considered in the book[39] and in a number of reviews.[16,28,40]

The above-considered investigation results concerning hardness, thermal stability, and oxidation of nanostructured films and the phase diagrams of these materials highlight a number of problems that call for further in-depth investigations. First of all, this is elucidating the regularities of diffusion in the nanocrystalline and amorphous films, which would provide better understanding of their thermal stability and corrosion resistance behaviors. The phase diagram predictions should take into account the specific thermodynamic behavior of nanosystems, this would increase the reliability of calculations and would stimulate experimental studies. Finally, extending the knowledge of the properties of interfaces in nanostructures is a necessary basis for the design of new nanostructured materials with higher levels of physicochemical, physicomechanical, and performance characteristics.

This work was supported by the Presidium of the Russian Academy of Sciences (Fundamental Research Programs No. 7 and 21).

References

1. Yu. D. Tret´yakov, E. A. Gudilin, *Usp. Khim.*, 2009, **78**, 867 [*Russ. Chem. Rev.*, (*Engl. Transl.*), 2009, **78**, 801].
2. I. V. Zibareva, A. V. Zibarev, V. M. Buznik, *Khimiya Ust. Razv.*, 2010, **18**, 215 [*Chem. Sustainable Development* (*Engl. Transl.*), 2010, **18**].
3. R. A. Andrievskii, I. I. Spivak, *Prochnost´ tugoplavkikh soedinenii i materialov na ikh osnove* [*Strength of Refractory Compounds and Materials Based on Them*], Metallurgiya, Chelyabinsk, 1989, 367 pp. (in Russian).
4. R. A. Andrievskii, *Zh. Vsesoyuz. Khim. o-va im. D. I. Mendeleeva*, 1991, **31**, No. 2, 137 [*Mendeleev Chem. J.* (*Engl. Transl.*), 1991, **31**, No. 2, 11].
5. R. A. Andrievski, *J. Mater. Sci.,* 1994, **29**, 614.
6. R. A. Andrievski, *Mater. Trans.*, 2001, **42**, 1471.
7. R. A. Andrievski, I. A. Anisimova, V. P. Anisimov, *Thin Solid Films*, 1991, **205**, 171.
8. R. A. Andrievskii, I. A. Anisimova, V. P. Anisimov, *Fiz. Khim. Obrabotki Materialov* [*Phys. Chem. Mater. Processing*], 1992, No. 2, 99 (in Russian).
9. R. A. Andrievskii, G. V. Kalinnikov, N. P. Kobelev, Ya. M. Soifer, D. V. Shtanskii, *Fiz. Tverd. Tela*, 1997, **39**, 1859 [*Sov. Phys. Solid State* (*Engl. Tansl.*), 1997, **39**, 1661].
10. O. Knotek, R. Breidenbach, F. Jungblat, F. Lofler, *Surf. Coat. Technol.*, 1990, **43/44**, 107.
11. C. Mitterer, M. Rauter, P. Rodhammer, *Surf. Coat. Technol.*, 1990, **41**, 351.
12. S. Veprek, *Plasma Chem. Plasma Process*, 1992, **12**, 219.
13. U. Helmerson, S. Todorova, S. A. Barnett, J. Helmerson, L. Market, J. Greene, *J. Apll. Phys.*, 1987, **62**, 481.
14. M. Shinn, L. Hultman, S. Barnett, *J. Mater. Res.*, 1992, **7**, 901.
15. N. Dubrovinskaia, V. L. Solozhenko, N. Miyajima, *Appl. Phys. Lett.*, 2007, **90**, 01912.
16. R. A. Andrievskii, A. M. Glezer, *Usp. Fiz. Nauk*, 2009, **179**, 337 [*Physics — Usp.* (*Engl. Transl.*), 2009, **52**, 315].
17. S. Veprek, *J. Vac. Sci. Technol. Ser. A*, 1999, **17**, 2401.
18. S Veprek, M. G. D. Veprek-Heijman, in *Nanostructured Coatings*, Eds A. Cavaleiro, J. T. de Hosson, Springer, Berlin, 2006.
19. R. A. Andrievskii, G. V. Kalinnikov, A. E. Oblezov, D. V. Shtanskii, *Dokl. Akad. Nauk*, 2002, **384**, 1 [*Dokl. Phys.* (*Engl. Transl.*), 2002, **47**, 353].
20. R. A. Andrievski, G. V. Kalinnikov, in *Nanostructured Thin Films and Nanodispersion Strengthened Coatings*, Eds A. A. Voevodin, D. V. Shtansky, E. A. Levashov, J. J. Moore, Kluwer Academic Publishers, Dordrecht, 2004, p. 175.
21. G. V. Kalinnikov, R. A. Andrievskii, V. N. Kopylov, D. Louzguine, *Fiz. Tverd. Tela*, 2008, **50**, 359 [*Sov. Phys. Solid State* (*Engl. Transl.*), 2008, **50**, 374].
22. G. V. Kalinnikov, R. A. Andrievski, V. K. Egorov, *J. Nano Research*, 2009, **6**, 89.
23. R. A. Andrievskii, Z. M. Dashevskii, G. V. Kalinnikov, *Pis´ma v Zh. Tekhn. Fiziki*, 2004, **30**, No. 22, 1 [*Techn. Phys. Lett.* (*Engl. Transl.*), 2004, **30**, No. 11, 930].
24. R. A. Andrievski, I. A. Anisimova, V. P. Anisimov, V. P. Makarov, V. P. Popova, *Thin Solid Films*, 1995, **261**, 83.
25. R. A. Andrievskii, *Usp. Khim.*, 2002, **71**, 967 [*Russ. Chem. Rev.* (*Engl. Transl.*), 2002, **71**, 853].
26. D.-G. Kim, T.-Y. Seong, Y.-J. Baik, *Surf. Coat. Technol.*, 2002, **153**, 79.
27. L. Hultman, C. Mitterer, in *Nanostructured Coatings*, Eds A. Cavaleiro, J. T. de Hosson, Springer, Berlin, 2006.
28. E. A. Levashev, D. V. Shtanskii, *Usp. Khim.*, 2007, **76**, 501 [*Russ. Chem. Rev.* (*Engl. Transl.*), 2007, **76**, 501].
29. R. A. Andrievskii, A. V. Khachoyan, *Ros. Khim. Zh.*, 2009, **53**, No. 2, 4 [*Russ. J. Gen. Chem.* (*Engl. Transl.*), 2010, **80**, 555].
30. R. A. Andrievski, *Rev. Adv. Mater. Sci.*, 2009, **21**, 107.
31. I. D. Morokhov, L. I. Trusov, V. N. Lapovok, *Fizicheskie yavleniya v ul´tradispersnykh sredakh* [*Physical Phenomena in Ultradisperse Media*], Energoatomizdat, Moscow, 1984, 324 pp.
32. M. Kh. Shorshorov, *Ul´tradispersnoe strukturnoe sostoyanie metallicheskikh splavov* [*Ultradisperse Structural State of Metal Alloys*], Nauka, Moscow, 2001, 155 pp. (in Russian).
33. R. A. Andrievskii, I. A. Anisimova, *Neorgan. Mater.*, 1991, **27**, 1450 [*Inorg. Mater.* (*Engl. Transl.*), 1991, **27,** 1450].
34. R. A. Andrievskii, G. V. Kalinnikov, *Fiz. Khim. Stekla*, 2007, **33**, 483 [*Glass Phys. Chem.* (*Engl. Transl.*), 2007, **33**, 483].
35. R. A. Andrievskii, V. A. Lavrenko, J. Demison, M. Demison-Brut, G. V. Kalinnikov, A. D. Panasyuk, *Dokl. Akad. Nauk*, 2000, **373**, 60 [*Dokl. Phys. Chem.* (*Engl. Transl.*), 2000, **373**, 99].
36. A. S. Edelstein, R. C. Cammarata, *Nanomaterials: Synthesis, Properties and Application*, IOP, Bristol, 1998, 596 pp.
37. R. K. Gupta, R. K. Singh Raman, C. C. Koch, *J. Mater. Sci.*, 2010, **45**, 4884.
38. J. Musil, J. Vliek, P. Zeman, *Appl. Adv. Ceram.,* 2008, **107**, 148.
39. *Nanostructured Coatings*, Eds A. Cavaleiro, J. T. de Hosson, Springer, Berlin, 2006.
40. R. A. Andrievskii, *Fiz. Met. Metalloved.*, 2010, **110**, 243 [*Phys. Met. Metallogr.* (*Engl. Transl.*), 2010, **110**, 229].

Received March 4, 2011